Topics in Catalysis (2020) 63:1532–1544
https://doi.org/10.1007/s11244-020-01302-2

ORIGINAL PAPER

Catalysis by Imaging: From Meso- to Nano-scale

Yuri Suchorski[1] · **Günther Rupprechter**[1]

Published online: 2 July 2020
© The Author(s) 2020

Abstract
In-situ imaging of catalytic reactions has provided insights into reaction front propagation, pattern formation and other spatio-temporal effects for decades. Most recently, analysis of the local image intensity opened a way towards evaluation of local reaction kinetics. Herein, our recent studies of catalytic CO oxidation on Pt(hkl) and Rh(hkl) via the *kinetics by imaging* approach, both on the meso- and nano-scale, are reviewed. Polycrystalline Pt and Rh foils and nanotips were used as µm- and nm-sized *surface structure libraries* as model systems for reactions in the 10^{-5}–10^{-6} mbar pressure range. Isobaric light-off and isothermal kinetic transitions were visualized *in-situ* at µm-resolution by photoemission electron microscopy (PEEM), and at nm-resolution by field emission microscopy (FEM) and field ion microscopy (FIM). The local reaction kinetics of individual Pt(hkl) and Rh(hkl) domains and nanofacets of Pt and Rh nanotips were deduced from the local image intensity analysis. This revealed the structure-sensitivity of CO oxidation, both in the light-off and in the kinetic bistability: for different low-index Pt surfaces, differences of up to 60 K in the critical light-off temperatures and remarkable differences in the bistability ranges of differently oriented stepped Rh surfaces were observed. To prove the spatial coherence of light-off on nanotips, proper orthogonal decomposition (POD) as a spatial correlation analysis was applied to the FIM video-data. The influence of particular configurations of steps and kinks on kinetic transitions were analysed by using the average nearest neighbour number as a common descriptor. Perspectives of nanosized surface structure libraries for future model studies are discussed.

1 Introduction

A mechanistic understanding of catalytic processes on solid surfaces requires to reveal the correlative relationship between the catalyst structure and the reaction kinetics over a wide range of the length scales. On the nm-scale, the surface structure controls the adsorption, diffusion and interaction of adsorbates [1–3]. Catalytic light-off is initiated on the nm-scale as well [4], but proceeds by propagation of reaction fronts via the meso- to the macro-scale [5, 6]. The shape and the local environment of a supported nanoparticle are nano-scale properties, while the particle distribution as well as the support morphology, affecting reactant flow, are again related to the meso- and macro-scale [7–9]. The construction and function of the 3-way automotive catalytic converter is a prime example of how overlapping and matching length scales are vital for application [10].

✉ Yuri Suchorski
yuri.suchorski@tuwien.ac.at

[1] Institut für Materialchemie, Technische Universität Wien, Getreidemarkt 9, 1060 Vienna, Austria

Such length-scale duality is also well-reflected in the historical development of the surface science approach to catalysis. The first molecular-level studies of adsorption on well-defined single crystal surfaces in the 1960ies were followed by pioneering reaction studies on single crystal model catalysts at the end of the 1970ies [11, 12]. Approximately at the same time, B. Niewenuys and V. Gorodetskii carried out nm-scale studies of adsorption and reactions of CO, NO, H_2 and O_2 on nm-sized tips of platinum group metals (PGM) by *field emission microscopy* (FEM) [13, 14]. In parallel, N. Kruse was the first to apply *pulsed field desorption mass spectrometry* (PFDMS) to study the CO and H_2 reaction [15] and Ru oxidation on atomic scale [16]. Since then, nm-sized tips made of precious metals were used as samples in field emission based techniques, and are established models of catalytic nanoparticles. The nanotips reflect well the main properties of nanoparticles: the size and presence of plenty of nanofacets of different crystallographic orientation (Fig. 1a). Using field evaporation in ultrahigh vacuum (UHV), the nanotips can be prepared with a defect-free atomically perfect surface and crystallographically characterised with atomic resolution using *field ion microscopy*

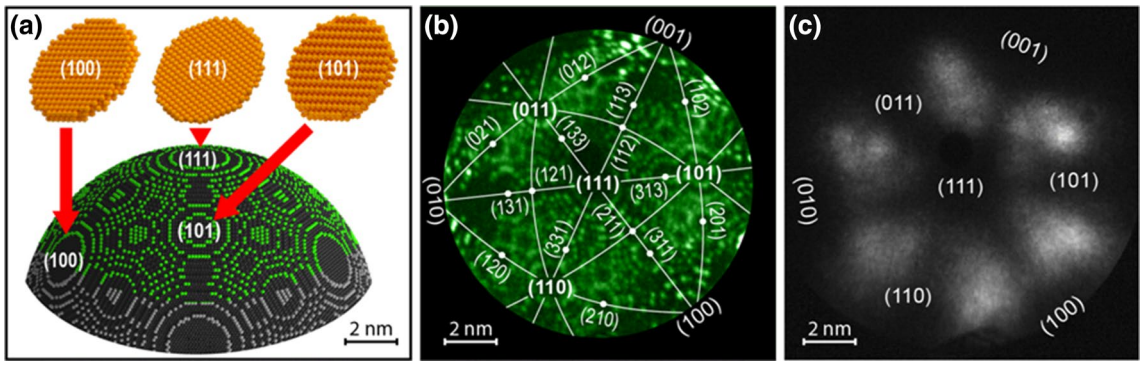

Fig. 1 PGM nanotip as a model of an individual catalytic nanoparticle: **a** ball model of an apex of an fcc nanocrystal; **b** Ne^+ FIM image of an [111]-oriented Rh tip superimposed with a stereographic projection of the crystallographic structure; **c** FEM image of the atomically-clean surface of the same tip. Adapted from Ref [19]. with permission from Springer

(FIM, Fig. 1b). An ongoing catalytic reaction can then be visualized in real-time using FEM or FIM and detailed information can be extracted from in-situ recorded video-files, as demonstrated for CO [17–19] and H_2 [20, 21] oxidation or NO_x reduction on Pt, Pd or Rh [22–24]. Furthermore, atom-probe (AP) techniques applied to the nanotips can provide surface and product analysis on an atomic scale [25, 26].

However, there is a gap in length-scale of 10^7 orders of magnitude between the (cm-size) single crystals and the nanotip-based systems. In addition, the reaction kinetics on single crystals is typically monitored by mass spectrometry (MS), averaging the data over macro-sized samples, whereas on the nanotips effects confined to individual nanofacets are accessible [27, 28].

Recently, we have used the domains of polycrystalline PGM foils, i.e. µm-sized single crystal surfaces combined in one sample, as scale-bridging model systems (Fig. 2). The prerequisites of such an application are the ability to crystallographically characterise each surface domain and to monitor the local reaction kinetics on the µm-scale [29]. The first task can be solved by *electron backscatter diffraction* (EBSD, Fig. 2b), and the second via the *local kinetics by imaging* approach [30], using which spatially-resolved kinetic data are extracted from video-files recorded by *in-situ photoemission electron microscopy* (PEEM, Fig. 2c), as explained below. The collection of different, but well defined µm-sized surfaces in "one-sample" serves as a *surface structure library*, consisting e.g. for a 10×10 mm^2 sample of hundreds of domains, often exposing high-Miller-index orientations particularly interesting for catalysis [19, 29]. Under certain conditions, such domains can behave independently in a surface reaction as was observed already in the 90ies [31], detecting oscillations in CO oxidation on Pt(110) and Pt(100) domains, while the (111)-type grains remained in a steady state, i.e. structure-dependent behaviour was directly observed.

Such surface structure libraries and nanotips are particularly suitable for studies of surface structure-sensitivity, since many different structures are simultaneously present in the field-of-view, under identical external parameters (p,

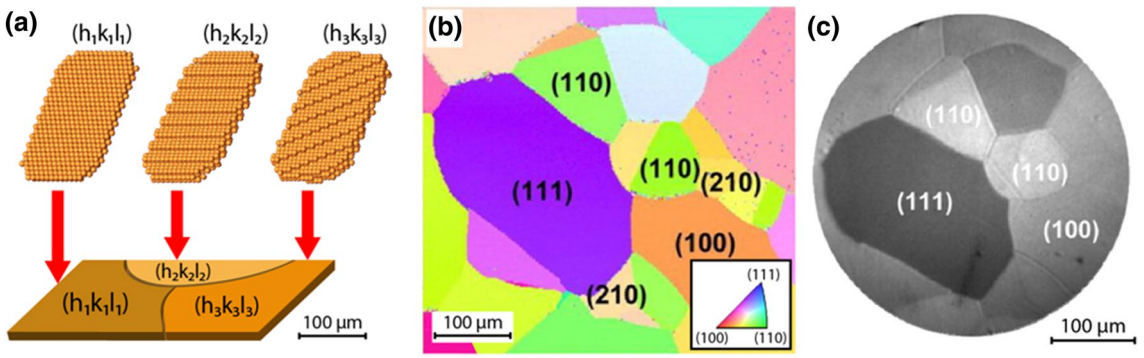

Fig. 2 Polycrystalline foil as surface structure library on the mesoscale: **a** the polycrystalline surface consists of differently oriented (hkl) domains; **b** determination of crystallographic orientations of individual Pd(hkl) domains by EBSD; **c** PEEM image of the same sample, differing work function values of different Pd(hkl) domains provide the image contrast. Adapted from Ref [29] with permission from Springer

T, T-ramps). The latter is difficult to fulfil in the traditional "one-structure-after-another" structure-sensitivity studies. In the present contribution, we focus on the advantages of both model systems, illustrated by recent PEEM and FEM/FIM studies of CO oxidation on Pt and Rh.

2 Experimental: Surface Structure Libraries and Local Kinetics by Imaging

For our meso-scale experiments, we operate an ultrahigh vacuum (UHV) apparatus as a flow reactor for CO oxidation, while the reaction is visualized in-situ by PEEM and video-recorded with a resolution of ~ 1 µm (Fig. 3a). The setup consists of two independent UHV chambers: (i) a PEEM-chamber with differential pumping (allowing in-situ studies at reactant pressures up to 10^4 mbar) and including sample preparation facilities, low energy electron diffraction (LEED), a mass spectrometer (MS), Auger electron spectroscopy (AES), gas supply, and (ii) an X-ray photoelectron spectroscopy (XPS) chamber with hemispherical electron energy analyser and Mg/Al X-ray gun (SPECS) and gas dosing allowing in-situ surface analysis. Both chambers are connected by a UHV sample transfer line.

The *local kinetics by imaging* approach for evaluation of reaction kinetics on individual domains of a polycrystalline sample is based on the fact that in a Langmuir–Hinshelwood reaction (such as CO oxidation on PGMs) the reaction rate is governed by the surface concentration (coverage) of adsorbed reactants. As the latter also determines the PEEM image via work function dependent emission of photoelectrons, there is a direct correlation between the local image intensity and the local reaction kinetics [30]. Due to the parallel imaging principle of PEEM, all regions in the field-of-view are imaged simultaneously (Fig. 3a). In combination with polycrystalline samples, this opens the unique possibility to directly compare the reaction kinetics of different (hkl)-domains, i.e. of different surface structures [4, 5, 19, 32, 33]. The same considerations are also valid for the FEM application to nanotips (Fig. 3b), because the FEM image created by field-emitted electrons is also governed by the local work function, with a certain contribution of local electric field variations. The local electric field depends on the surface structure, due to the local field enhancement above individual surface atoms [34], i.e. strongly corrugated surfaces will appear "brighter" in a FEM. However, due to the Smoluchowski effect [35], such surfaces also have lower work function (higher electron emission at the same field), thus the relationship between surface coverage and image intensity is still valid.

In the present FIM studies, in which the image is created by O_2^+ species field-ionized at the imaged surface, the work function contributes as well, by influencing the critical distance of field ionization and thus the probability of field ion formation [36, 37]. In this particular case of O_2^+ FIM, resonance field ionization of oxygen also contributes to the image contrast [38] and the atomic scale roughness of the surface also has a specific, but well-studied, effect via local electric field variations [34, 37]. This allows the application of the *kinetics by imaging approach* down to the nm-scale, and enables the comparison of nm-sized facets with corresponding µm-sized domains.

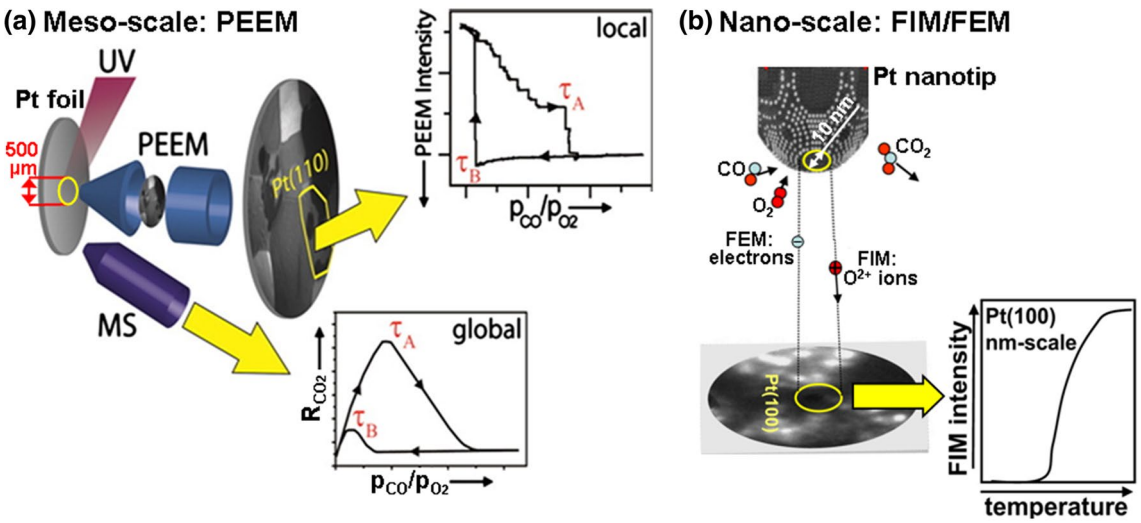

Fig. 3 Experimental approach: **a** An ongoing catalytic reaction on a polycrystalline sample (µm-scale) is monitored simultaneously by PEEM and MS. Local data obtained from the intensity analysis of PEEM video-sequences for each individual (hkl)-domain are compared with global (averaged) MS data; **b** A nanotip is used as sample and the reaction is monitored on the nm-scale by FEM or FIM, using electrons or O^{2+} ions as imaging species, respectively. Adapted from References [4, 30] with permission from Springer and Elsevier

For FEM/FIM studies, a separate UHV apparatus was used containing a cooled/heated (77–1500 K) nanotip holder and a channel-plate/screen assembly. The apparatus is equipped with gas supply for reactive (CO, H_2, O_2) and noble (He, Ne, both for FIM imaging) gases, and was newly upgraded by a novel, recently developed temperature control system, based on wireless data transmission between the control panel and the high-voltage facilities [39].

3 CO Oxidation on Pt: Structure Sensitivity and Coupling in Catalytic Light-off

Surface structure libraries are exceptionally well-suited for investigations of the structure sensitivity of catalytic light-off of CO oxidation on Pt. When a polycrystalline Pt surface is heated (temperature ramp) in a CO/O_2 mixture and simultaneously monitored by PEEM, the Pt(hkl) domain at which light-off occurs first (i.e. at lowest temperature) becomes directly visible. Such observations are important for pollution control: the lower the light-off temperature is, the less CO is emitted during the cold start of an engine. Reducing the light-off temperature may serve as an energy neutral alternative to sophisticated car catalyst heating devices developed in order to fulfil today's stringent emission standards [4, 40], and references therein.

The experiment is illustrated in Fig. 4, in which catalytic light-off is visible in PEEM as nucleation of "dark" catalytically active O-covered regions on specific Pt(hkl) domains. They appear "dark" since adsorbed oxygen increases the work function of Pt, therefore the O-covered regions emit less photo-electrons than the clean or CO-covered Pt surface. The O-covered surface is active in CO oxidation, because a relatively open layer of adsorbed O-atoms (e.g. 2×2 on Pt(111) [3]) allows CO to adsorb in between and react. In turn, a densely-packed CO layer with carbon bonding "on-top" of Pt atoms [3], prevents oxygen adsoption due to the lack of pairs of free adsorption sites necessary for dissociative oxygen adsorption. In this way, the CO covered surface remains catalytically inactive until the increasing temperature initiates CO desorption. This shifts the co-adsorption equilibrium in favour of oxygen and causes a kinetic phase transition to the active regime, initiating so the light-off.

In this description we refrain from light-off related heat generation/dissipation problems in an exothermal reaction [41], as they play a minor role in UHV experiments on model systems.

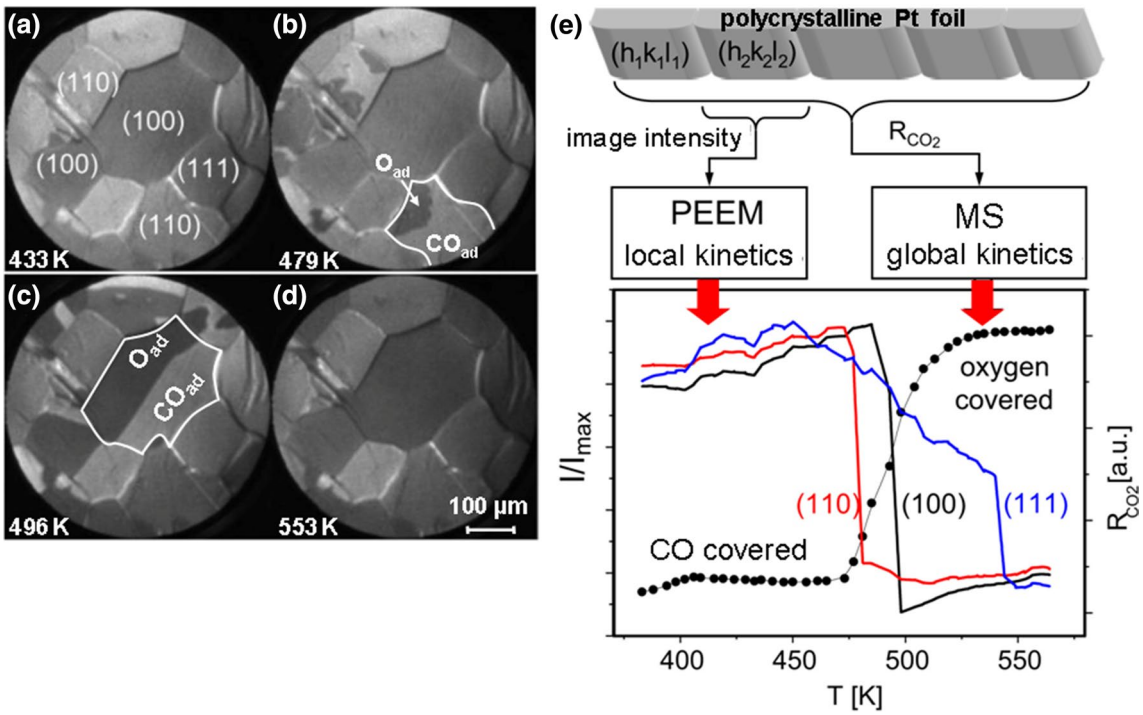

Fig. 4 Structure sensitivity of the light-off in CO oxidation on Pt: **a**–**d** PEEM video-sequence recorded at constant $p_{CO}=6.6\times10^{-6}$ mbar and $p_{O2}=1.3\times10^{-5}$ mbar during a temperature ramp of ~0.5 K/s from 385 to 565 K. Frame **a** shows the inactive CO-covered surface as it appears until the light-off begins. Frame **b** catalytic light-off starts: dark O_{ad}-covered areas nucleate and spread over the (110)-domains. Frame **c** light-off is visible on the (100)-domains. Frame **d** after completed light-off, the whole field of view shows the active O-covered surface. **e** Evolution of the local PEEM intensity for Pt(110), Pt(100) and Pt(111) domains during the light-off process. For comparison a global R_{CO2} curve measured in parallel by MS is shown. Adapted from Reference [4] with permission from Elsevier

The PEEM observation presented in Fig. 4 evidences the structure sensitivity of light-off in CO oxidation: local ignitions do not occur simultaneously for the different orientations, but clearly show different critical temperatures: 480 K for Pt(110), 496 K for Pt(100), and 542 K for Pt(111) deduced as inflection points of corresponding local PEEM intensity curves. In contrary, the global CO_2 production rate, R_{CO2}, measured simultaneously by MS shows a smoothened shape, emphasizing the main drawback of conventional mass spectrometry: averaging over the whole sample consisting typically of differently active regions. Analysis of PEEM video-files provides, in turn, local light-off behaviour on a µm-scale and clearly identifies the Pt(110) surface as that with the lowest critical temperature among the low Miller index planes of Pt. In PEEM, local ignitions are manifested by reaction fronts which nucleate usually at grain boundaries (Fig. 4b) or defects [42], and then spread over the entire domain (Fig. 4c), but remain confined by the grain boundary [5, 42, 43], at least under the present or similar conditions. The facts, that the front propagation remains confined and that the gas coupling can be neglected under the present UHV conditions, allowed the conclusion that individual (hkl) domains exhibited independent reaction properties, analogous to the corresponding single crystals [5, 42, 43].

For nm-scale studies, an [100]-oriented Pt nanotip was used and the light-off in CO oxidation was monitored by FIM. As mentioned, the origin of FIM image contrast is more complex than in PEEM (for which the work function directly governs the photoelectron yield). Despite this complexity, the FIM image contrast of the CO/O/Pt system is well understood: when imaging with O^{2+} ions, the CO-covered areas always appear darker than the corresponding O-covered regions [37, 38]. Consequently, the FIM images of ongoing CO oxidation on Pt appear as "negatives" of PEEM images, but the active and inactive states can still be discriminated reliably.

Figure 5a shows a sequence of six consecutive FIM images recorded during light-off in CO oxidation on a [100]-oriented Pt nanotip which exhibits, among many others, the main low Miller-index planes, in analogy to the polycrystalline Pt sample of Fig. 4. The positions of the regions of interest (ROIs) placed on Pt(100), Pt(110) and Pt(111) facets are indicated in frame 1 of Fig. 5a.

A visual inspection of video-files and a local intensity analysis of the ROIs placed on low-index planes (Fig. 5b) create the impression that ignition occurs in a spatially-coherent way over the majority of the facets. To prove this impression quantitatively, we applied orthogonal decomposition (POD) as spatial correlation analysis to the video-FIM data, also known as Karhunen-Loève transformation. POD analysis is a powerful method of data analysis able to reliably detect coherent spatio-temporal modes, e.g. in hydrodynamics [44, 45]. We have previously applied POD for the analysis of reaction-induced fluctuations [46] and

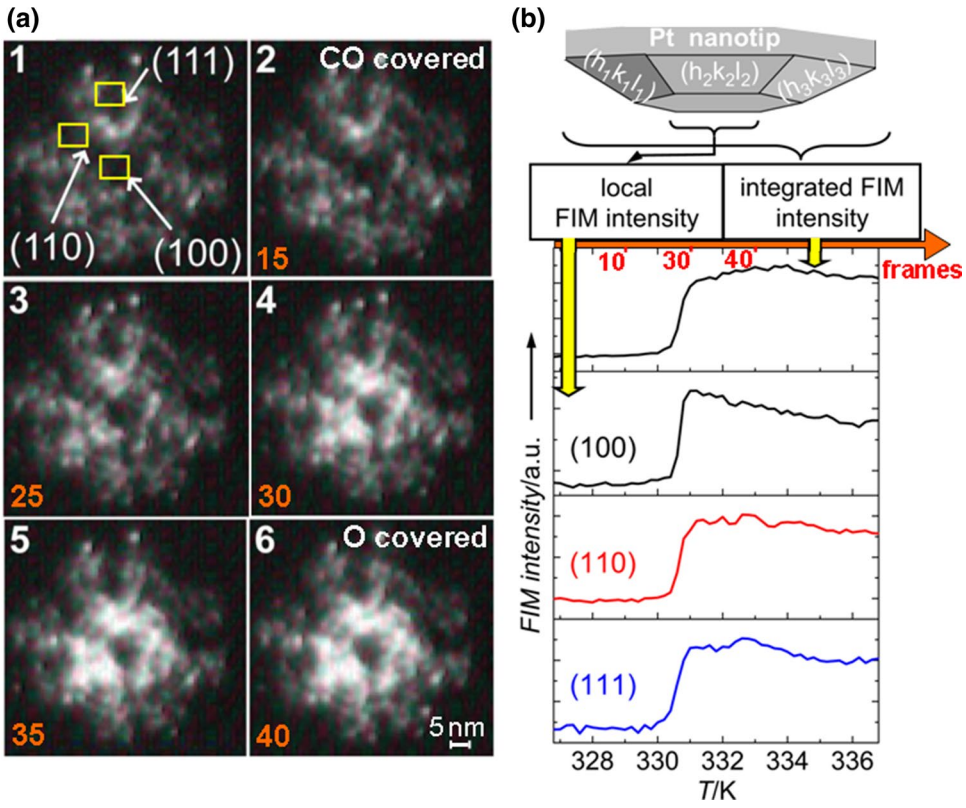

Fig. 5 Light-off in CO oxidation on a [100]-oriented Pt nanotip as monitored by FIM: **a** Sequence of selected FIM images recorded *in-situ* during a temperature ramp from 325 to 340 K at constant $p_{CO} = 5.3 \times 10^{-7}$ mbar and $p_{O2} = 5.3 \times 10^{-4}$ mbar (red frame numbers correspond to the red frames-axis in (b)). The positions of ROIs placed on the low Miller-index facets are shown in the first frame. Bright areas in frames 4–6 are catalytically active O_{ad}-covered regions; **b** FIM intensity integrated within the field of view (upper curve) and within the ROIs (lower curves) placed on (100), (110) and (111) facets, plotted *versus* temperature. Adapted from Reference [4] with permission from Elsevier

for proving the spatial desynchronization of glycolytic waves [47].

The idea of POD is based on the fact that any spatio-temporal signal $w(x,t)$ can be decomposed into *time-dependent* amplitudes $a_n(t)$ and *time-independent* modes $b_n(x)$ which form an orthogonal basis, i.e.: $\omega(\mathbf{x},t) = \sum a_n(t) b_n(\mathbf{x})$. The basis functions $b_n(x)$ are *eigenvectors* of the equation $\mathbf{S}\cdot b_n(x) = \Lambda_n \cdot b_n(x)$, in which Λ_n are *eigenvalues* and $\boldsymbol{S}$ is the correlation matrix. Each eigenvalue Λ_n denotes the weight of the corresponding eigenvector $b_n(x)$, *i.e.* the variance of the original data set projected along this eigenvector.

The POD analysis of the light-off process shown in Fig. 5 is presented in Fig. 6a, in which a set of the original FIM video-frames (left column) is compared with the POD reconstruction (right column), performed using solely the first POD mode. The images in the right column, reconstructed from the first eigenvector (constant spatial picture $b_1(x)$ multiplied with the calculated time-dependent amplitude $a_1(t)$, the latter shown in Fig. 6b, upper panel), mimic well the original video-signal. This clearly demonstrates that already the first POD mode, containing in the present case 86% of the entire signal weight, captures well the light-off process. The higher modes contributed only little to the overall dynamics of the system. This indicates a high degree of spatial correlation, i.e. the light-off occurs in a *synchronized* way for all surface orientations of the nanotip. This is also evident from Fig. 6b, in which the reconstructed time-dependent amplitude of the first POD mode is compared with the integrated experimental FIM intensity.

This is in contrary to the observations on the µm-sized Pt(hkl) domains for which an independent behavior of the individual domains was observed (Fig. 4). The observed differences shed light on the spatial coupling in CO oxidation: since the thermal coupling and the gas phase coupling (or rather its absence under the present UHV conditions [4, 5]), are similar for the foil and nanotip, only diffusion coupling via surface CO supply can be responsible for the observed effects, since the diffusion of the much less mobile adsorbed O-atoms can be neglected under the present conditions [48]. In fact, the diffusion length of CO reaches the µm-range under the present reaction conditions [48, 49], i.e. exceeding the size of nanofacets on the nanotip by orders of magnitude and resulting in synchronous light-off on all tip facets in the field of view. The fact that light-off on each µm-sized Pt(hkl) domain occurs independently, decoupled from other domains, agrees well with the observation that reaction fronts originating from pressure variations at constant temperature are confined within grain boundaries [50]. Thus, the present light-off data obtained for Pt(hkl) domains (Fig. 5) should also be valid for single crystals of the same orientation.

4 CO Oxidation on Rh: Surface Sensitive Bistability and Role of Stepped Surfaces

The catalytic properties of nanoparticles strongly depend on their size, shape and the atomic arrangement of their confining surfaces. For example, high-Miller-index PGM surfaces

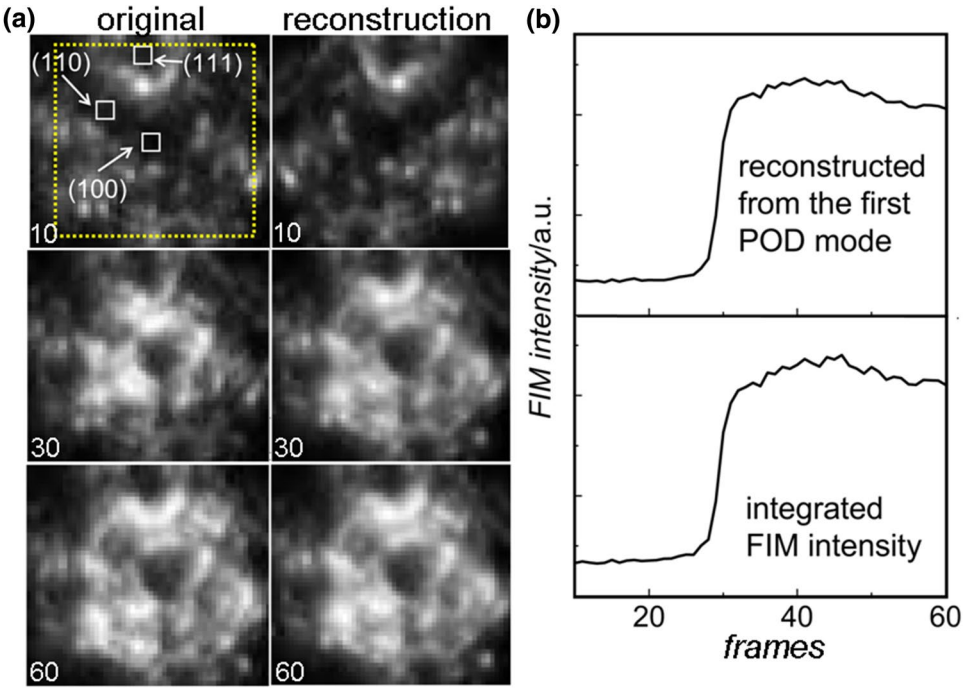

Fig. 6 POD analysis of light-off in CO oxidation on a [100]-oriented Pt nanotip: **a** Selected original FIM video-frames (left column) and the POD reconstruction using the first POD mode (right column). The region used for the POD analysis is marked by the yellow dotted line. ROI positions for individual orientations (the same as in Fig. 5a) are indicated; **b** Upper curve: FIM intensity reconstructed as time-dependent amplitude of the first POD mode containing 86% of the total signal. Lower curve: original FIM intensity integrated within the POD region marked in (**a**). Experimental conditions correspond to that of Fig. 5. Adapted from Reference [4] with permission from Elsevier

rich in steps and kinks, often exhibit higher catalytic activity than low-index planes of densely packed atoms [51, 52]. To guide nanoparticle synthesis, one needs to know which stepped surfaces are most active, i.e. one needs to study reactions on high-Miller-index facets to identify the most promising.

Polycrystalline foils containing hundreds of µm-sized stepped surface domains and nanotips exhibiting nm-sized stepped facets are again well-suited for such studies. Different structures are exposed to the very same p/T conditions at a time, making a direct comparison of different crystallographic orientations straightforward. We focus on CO oxidation on Rh, as it is increasingly used for the newest generation of automotive catalytic converters, designed for direct injection gasoline engines working under lean-burn conditions (e.g. "four way catalyst" by BASF [53]) and for purification of the hydrogen feed of proton-exchange membrane fuel cells by preferential CO oxidation [54]. Reaction data for high-Miller-index Rh surfaces are scarce, since previous research mostly focused on low-index planes [55–57], including a vivid debate about the structure-sensitivity of the reaction [58–60]. We used a polycrystalline Rh foil as library of highly stepped surfaces and again applied PEEM to image CO oxidation in-situ (Fig. 7, note that contrary to Pt, on Rh

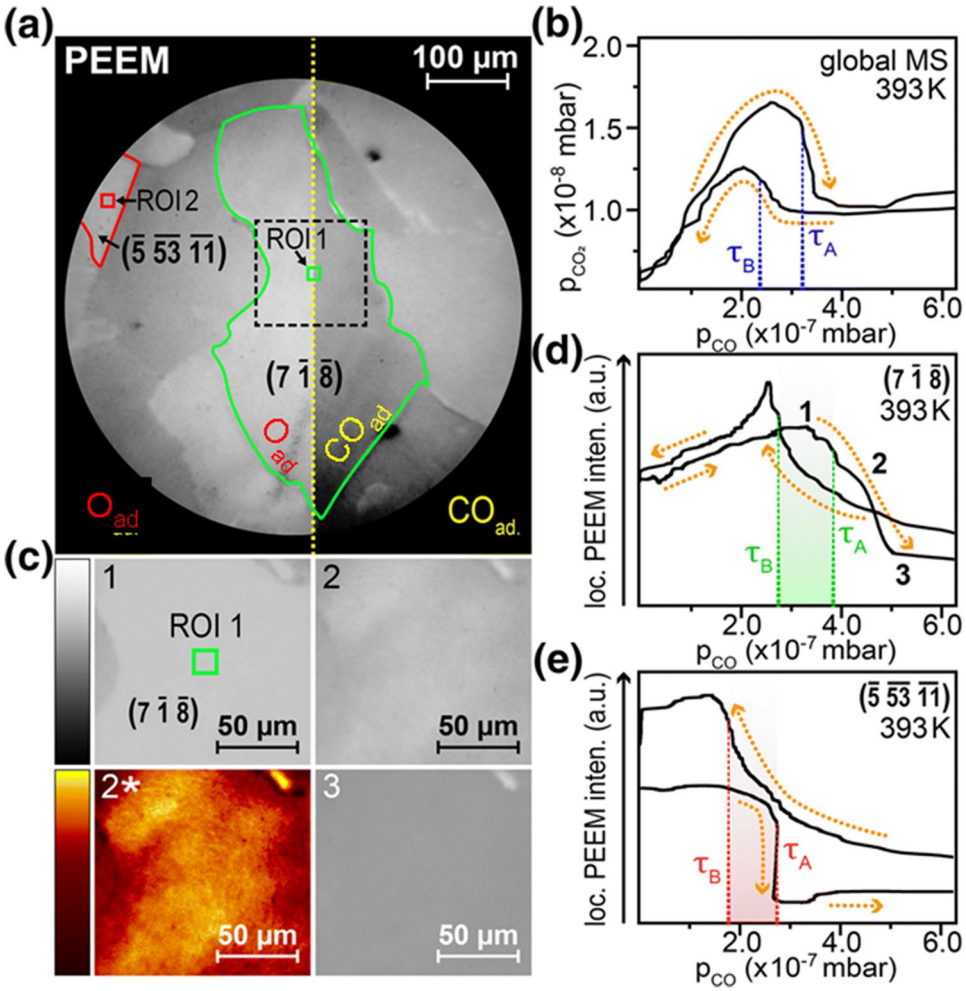

Fig. 7 CO oxidation on Rh: **a** Image of the PEEM field of view composed of two half-frames: the left half shows the O-covered Rh surface, the right half the CO-covered surface (always darker in comparison to the same, but O-covered surface, *cf.* left and right halves of $(7 \cdot \bar{1} \cdot \bar{8})$ domain). The Rh$(7 \cdot \bar{1} \cdot \bar{8})$ and Rh$(\bar{5} \cdot \bar{53} \cdot \bar{11})$ domains and corresponding ROIs are marked in green and red, respectively; **b** hysteresis in the global CO_2 production rate as measured by MS during cyclewise variation of p_{CO} at constant $p_{O2} = 1.0 \times 10^{-6}$ mbar and 393 K; **c** PEEM video-frames taken during the kinetic transition τ_A within the square region (dashed line) on the Rh$(7 \cdot \bar{1} \cdot \bar{8})$ domain in (**a**). Frame 1: O-covered surface; frame 2: during the kinetic transition τ_A; frame 2*: the same as frame 2, but color-coded instead of grey scale. The grey scale and the corresponding color code are shown on the left of frames 1 and 2*, correspondingly; frame 3: CO-covered surface; **d** hysteresis in the local PEEM intensity measured within ROI 1 (green square within Rh$(7 \cdot \bar{1} \cdot \bar{8})$ domain). The numbered positions on the hysteresis curve correspond to the frame numbers in (**c**); **e** the same but for the Rh$(\bar{5} \cdot \bar{53} \cdot \bar{11})$. Adapted from Reference [19] with permission from Springer

the CO covered surface appears darker than the corresponding O-covered surface [19]). The global CO_2 production was monitored in parallel by MS.

The differing adsorption kinetics of CO and O_2 mentioned above (CO inhibits the adsorption of oxygen, but not vice versa) leads to a kinetic bistability in catalytic CO oxidation on PGMs, leading to two different stable steady-states at the same set of external parameters [3, 61]. Solely the system prehistory determines which of the two steady-states (high or low catalytic activity) prevails: the high activity state is accessed from the oxygen excess regime, whereas the inactive state is reached from the CO excess regime. The bistability shows up as a hysteresis of the reaction rate upon cyclic variation of control parameters, e.g. the CO pressure (at constant p_{O2} and T) [62]. Figure 7 illustrates this behaviour for polycrystalline Rh: at low CO pressures, the Rh surface is O-covered and increasing the CO pressure leads to an increased R_{CO2} until a kinetic phase transition occurs at $p_{CO} = \tau_A$, manifested by a drop in R_{CO2} (Fig. 7b). It is caused by the sudden loss of catalytic activity due to switching from the O-covered to the CO-covered surface, as visible in PEEM (Fig. 7a, d, e). At subsequently decreasing p_{CO}, the Rh surface remains in the CO poisoned (low activity) state until a second kinetic transition (return to the active O-covered surface) takes place at $p_{CO} = \tau_B$ (Fig. 7b). PEEM allows not only to differentiate active and inactive surfaces, but also reveals the surface sensitivity of kinetic transitions: e.g. the local PEEM image intensity of ROI 1 located within the Rh$(7 \cdot \bar{1} \cdot \bar{8})$ domain draws a hysteresis, similar as R_{CO2} does, but the position of this local hysteresis (Fig. 7d) is different from that of the global MS measurements. Analogously, Fig. 7e shows the hysteresis measured locally for the Rh$(\bar{5} \cdot \overline{53} \cdot \overline{11})$ domain, which differs from both the hysteresis observed for Rh$(7 \cdot \bar{1} \cdot \bar{8})$ domain and that measured globally by MS.

This directly proves the structure dependence of CO oxidation on stepped Rh surfaces, significantly extending the previous findings for low-index planes. An interesting feature observed by PEEM is the formation of cellular-like structures (frame 2 in Fig. 7c): small short-living islands (better visible in the color-coded frame 2*) nucleate, creating a fluctuating turbulent picture during the kinetic transition. These structures formally resemble the patterns observed by Rose et al. during CO oxidation on Pt(110) by mirror electron microscopy (MEM) [63], but they differ by much faster temporal evolution (tens of µs in the present case *vs*. few s in Ref. [63].). The authors of [63] associated the observed cellular structures with the formation of CO islands on Pt(110), which seems to be in accordance with the present observations. Indeed, on Pt(110) cellular-like structures were visible in regions containing step-bunches and also our Rh surface was a high-Miller-index stepped surface. This interpretation is also in agreement with our previous nanoscale study [28], in which a drastic increase in the size of nucleating CO islands (from nm to µm scale) due to increasing correlation length of reaction-induced fluctuations was predicted for certain conditions in the bistable range of the reaction. Unfortunately, the limited spatial and temporal resolution of the employed PEEM, do not allow judging whether the formation of the observed short-lived cellular patterns is related to this effect. Alternatively, the combination of reaction-induced microscopic roughening, as observed for Pt(110) in [64], and the varying substrate dependent binding sites of CO influencing the spatial pattern formation [65], could cause the observed phenomenon.

Reaction fronts, often observed for CO oxidation on low index Pt and Pd surfaces [3, 5, 50], were not observed for Rh. To our knowledge, mesoscopic fronts were not yet directly observed during CO oxidation on Rh under high vacuum conditions. Microscopic fronts, however, were observed by STM in titration experiments on Rh(110) [66].

Apart from Rh$(7 \cdot \bar{1} \cdot \bar{8})$ and Rh$(\bar{5} \cdot \overline{53} \cdot \overline{11})$ domains, also Rh$(\overline{30} \cdot 37 \cdot \bar{6})$, Rh$(\bar{2} \cdot 0 \cdot 3)$, Rh$(\bar{1} \cdot 8 \cdot 18)$, and Rh$(\bar{3} \cdot 1 \cdot 24)$ domains were in the PEEM field of view. To compare all these orientations, we used a kinetic *phase diagram* (logarithmic plots of τ_A and τ_B values *versus* the reciprocal temperature), in which the steady state regions and the region of bistability are marked. Figure 8a shows such diagrams for different stepped Rh(hkl) domains visible in the field of view in Fig. 7a, for constant O_2 pressure of 1.0×10^{-6} mbar and for a temperature interval of 393–458 K.

The diagrams in Fig. 8 demonstrate that such structural factors as density of steps (related to the width of the terraces), the structure of terraces and the shape of the steps influence the relative position of a diagram. In a simple quantitative approximation, these factors can be united in the average nearest neighbour number as a common descriptor. For illustration, in Fig. 8c, the transition pressure τ_A, which reflects the tolerance of the system towards CO poisoning, is plotted versus the average nearest neighbour number. The plot reveals a clear correlation for an exemplary temperature of 413 K: the lower the average coordination of surface atoms is, the more CO is necessary to poison the surface, i.e. the rougher surfaces are the "better" catalysts.

To directly compare the µm- and nm-scale behaviour of CO oxidation on stepped Rh surfaces, the reaction was studied by FEM on a Rh nanotip. Catalytic experiments were performed in the same manner and under the same conditions as for the polycrystalline Rh foil.

Figure 9a shows FEM video frames illustrating the kinetic transitions τ_A and τ_B during the cyclewise variation of the CO pressure at constant $p_{O2} = 1.0 \times 10^{-6}$ mbar and T = 403 K. The resulting hysteresis loop and the resulting kinetic phase diagram are shown in Fig. 9b, c. Kinetic phase diagrams are not only suitable to compare catalytic behaviour of differently oriented domains of the same

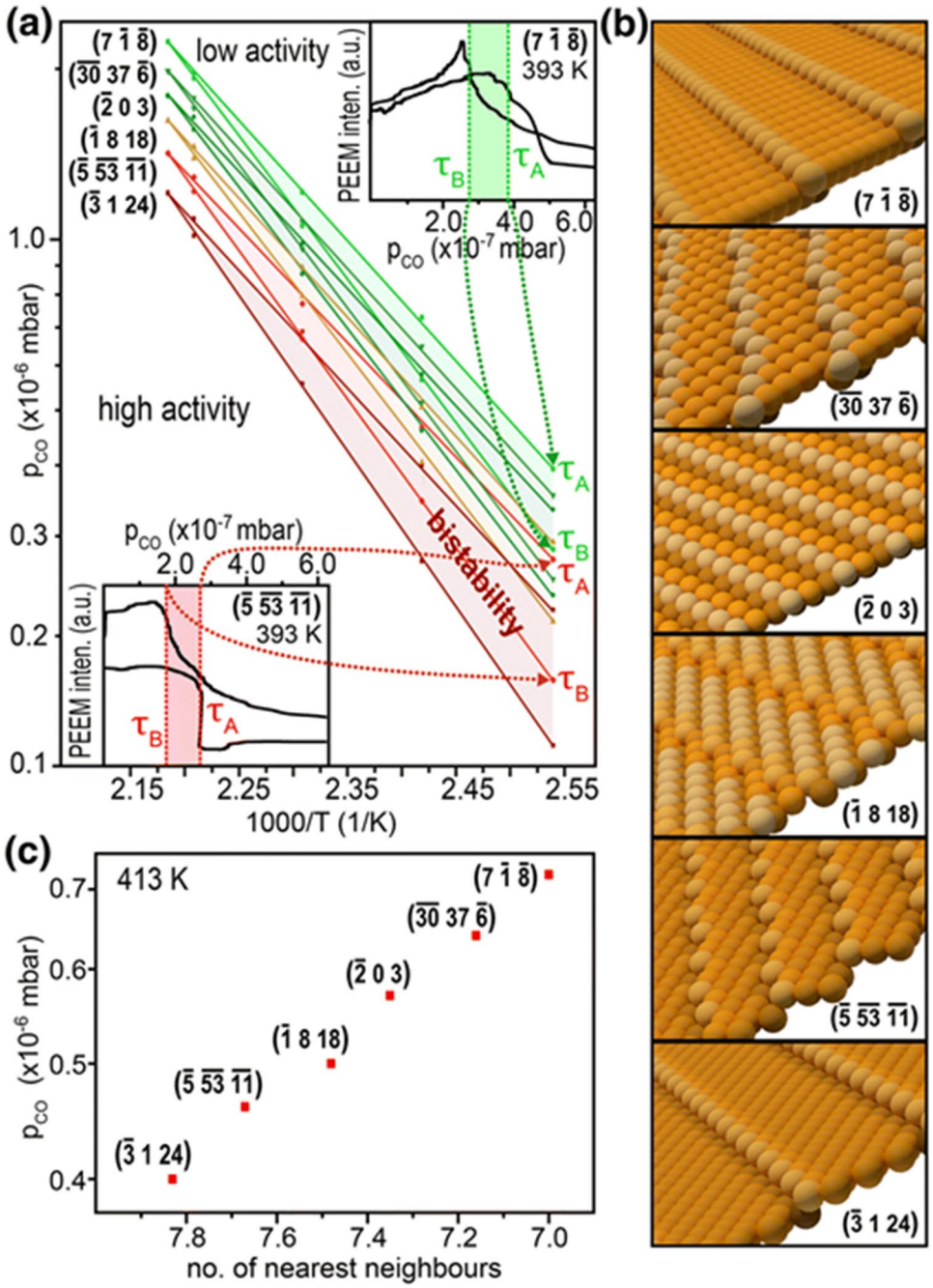

Fig. 8 Structure sensitivity of CO oxidation on differently oriented high-Miller-index Rh surfaces: **a** kinetic phase diagrams for individual domains visible in the PEEM field of view; **b** surface structures corresponding to particular Rh(hkl) domains; **c** position of the kinetic transition τ_A in dependence of the average number of nearest neighbours. Reproduced from Reference [19] with permission from Springer

sample (as e.g. in Fig. 8a), but also to compare different systems under similar conditions, in the present case a polycrystalline Rh foil and a Rh nanotip. The comparison in Fig. 10 reveals that the bistability region of the Rh nanotip is significantly shifted to higher CO pressure (by a factor of ~ 3). This indicates that on the nanotip reaction inhibition by CO requires considerably higher CO partial pressure (higher CO tolerance) and that the tip surface is also reactivated at a higher CO pressure than the Rh foil. Accordingly, the Rh nanotip is a better CO oxidation catalyst than the Rh foil, both on average but also for each individual µm-sized high-Miller-index Rh domain.

For better understanding of the above results, a Rh foil sample with a step density close to that of the Rh tip surface was prepared by Ar^+ sputtering (*cf.* our recent STM observation of the Ar^+ created steps and defects on Pd [50]). The phase diagram of such an artificially defected Rh surface was also shifted to higher CO pressures as compared the annealed high-Miller-index Rh domains, but was still located in between annealed foil and Rh nanotip

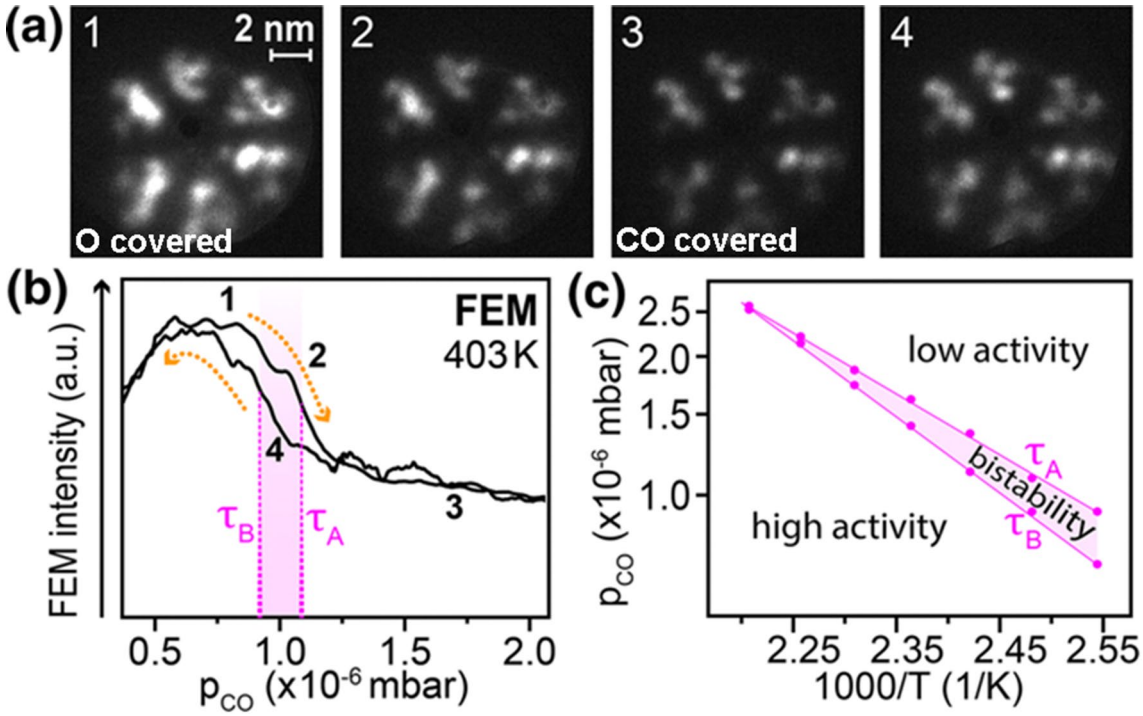

Fig. 9 CO oxidation on a Rh nanotip: **a** selected FEM video frames taken during cyclewise variation of p_{CO} at constant $p_{O2} = 1.0 \times 10^{-6}$ mbar and T = 403 K; **b** corresponding hysteresis-like curve of the FEM image intensity; τ_A and τ_B mark the kinetic transitions between the steady states of low and high catalytic activity, the numbers on the curve correspond to the frames in (**a**); **c** τ_A and τ_B values for different temperatures in the range of 393–453 K and constant oxygen pressure of 1.0×10^{-6} mbar, summarised in a kinetic phase diagram. Reproduced from Reference [19] with permission from Springer

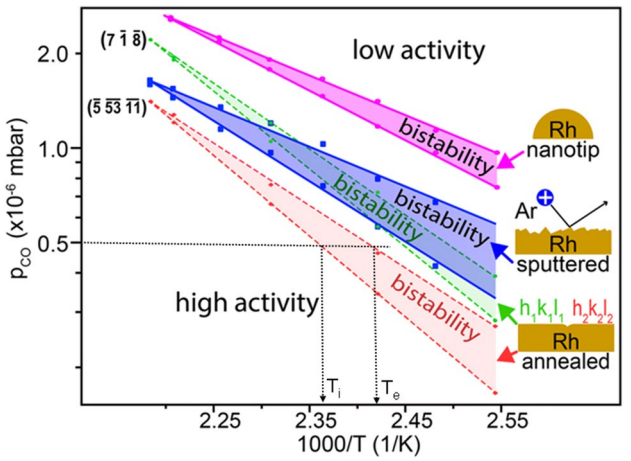

Fig. 10 Comparison of the kinetic phase diagrams for CO oxidation on two different annealed Rh(hkl) domains (dashed green and red), on the same but additionally Ar^+ sputtered foil (blue) and on a Rh nanotip (pink). All diagrams were constructed for constant $p_{O2} = 1.0 \times 10^{-6}$ mbar. Dotted horizontal line at $p_{CO} = 0.5 \times 10^{-6}$ mbar exemplarily shows the extraction of the predicted ignition and extinction temperatures T_i and T_e. Reproduced from Ref [19] with permission from Springer

(Fig. 10). The equivalence of isobaric and isothermal experiments demonstrated in our previous studies [5, 67] allows to predict the ignition and extinction temperatures from kinetic phase diagrams, as schematically shown in Fig. 10 (see detailed explanation in Ref [5].). In the present case this means that ignition and extinction temperatures will be shifted to lower temperatures for the sputtered (rougher) Rh surface with respect to the annealed (flatter) Rh surfaces. This effect was already detected earlier for Pd under similar conditions [5] and was also observed under more realistic NAP conditions, when for a stepped Pd surface the ignition/extinction loop was shifted to lower temperatures as compared to smooth Pd(111) [68].

To rationalize the above findings, we remind that the binding energy of oxygen at low-coordination defect sites is considerably higher than that on flat terraces of Rh, that is, atomic oxygen binds stronger to a defect-rich Rh surface [69, 70]. Although the CO binding energy is also increased on such defect sites [71], the impact on the CO adsorption kinetics seems to be rather small when compared to oxygen. Since the energetics governs the kinetics of the competitive CO and oxygen coadsorption [67], this explains why higher CO pressure is required to poison the surface on sputtered Rh.

Nevertheless, this does not explain the remarkable difference between a sputtered Rh foil and a Rh tip consisting mainly of stepped nano-facets. Apparently, reaction-induced fluctuations, which have significant effect on kinetic transitions in nm-sized reaction systems [27, 28], shift the whole phase diagram of a Rh nanotip to higher CO pressures. Interestingly, recent studies of catalytic H_2 oxidation have also shown that the Rh nanotip exhibited higher activity than sputtered and annealed Rh foils [33].

5 Summary and Outlook

Catalysis on solid surfaces is a prime example for the manifold correlations between microscopic properties and spatio-temporal effects on the meso-scale, such as reaction front propagation and pattern formation. This proves the necessity of combined µm- and nm-scale studies of the *same* reaction on the *same* surface structures under the *same* reaction conditions. Our recent studies summarized here, followed this idea, exemplified by CO oxidation on Pt(hkl) and Rh(hkl) both on the meso- and nano-scale.

For mesoscale studies we used µm-sized domains of polycrystalline samples as model systems and in-situ PEEM imaging as method for extracting local kinetic data. The polycrystalline samples containing plenty of different crystallographic orientations served as *surface structure libraries*. This allowed us to reveal the structure sensitivity of CO oxidation, both in the light-off and in the kinetic bistability. For different low-index Pt surfaces, differences of up to 60 K in the critical light-off temperatures and remarkable differences in bistability ranges of differently oriented stepped Rh surfaces were observed.

For nanoscale studies, nm-sized Pt and Rh tips, containing nanofacets of the same orientations as the polycrystalline foils, were used as samples and FEM/FIM for imaging. This provided insights into the role of spatial coupling and facet-size-effects on bistability and light-off in nanosized systems. The apices of nanosized tips made from catalytically active materials can also be considered as surface structure libraries, but in the nm-range and with the advantage that the size of individual nanofacets can be deliberately varied by using tips of different radii. Even differently-sized facets of the same orientation can be formed *on one tip*, as demonstrated in [28]. This allows to study size effects, particularly their role in fluctuation induced phenomena, a topic already touched in pioneering studies [27, 28], but still awaiting its further exploration, particularly for reactions other than CO oxidation. The interesting property of such nanotips is that the characteristics of fluctuations, e.g. their bimodality, are confined within the particular nm-sized facet, despite the absence of grain boundaries. This turns such tips into unique model systems, allowing studying effects not accessible to other methods. The parallel imaging principle of FEM/FIM plays a crucial role here, because all surface sites *simultaneously* emit information carriers (electrons or ions, respectively), which allows to apply sophisticated analysis tools such as POD, based on calculations of spatial correlations. One should further note that the tip facets consist mainly of stepped and kinked surfaces, which are considered to exhibit the catalytically most active sites. An intense atomic scale characterization of these exceptional surface sites and the systematic correlation of the local characteristics with local kinetic reaction parameters, both on the nano- and meso-scale, seems to be a promising way towards a deeper understanding of the mystery of "active sites".

Acknowledgements Open access funding provided by Austrian Science Fund (FWF). This work was supported by the Austrian Science Fund (FWF) via projects P 32772-N and SFB-F4504/02-FOXSI.

Compliance with Ethical Standards

Conflict of interest The authors declare that they have no conflict of interest.

Open Access This article is licensed under a Creative Commons Attribution 4.0 International License, which permits use, sharing, adaptation, distribution and reproduction in any medium or format, as long as you give appropriate credit to the original author(s) and the source, provide a link to the Creative Commons licence, and indicate if changes were made. The images or other third party material in this article are included in the article's Creative Commons licence, unless indicated otherwise in a credit line to the material. If material is not included in the article's Creative Commons licence and your intended use is not permitted by statutory regulation or exceeds the permitted use, you will need to obtain permission directly from the copyright holder. To view a copy of this licence, visit http://creativecommons.org/licenses/by/4.0/.

References

1. Rioux RM, Song H, Yang P, Somorjai GA (2008) Platinum nanoclusters size and surface structure sensitivity of catalytic reactions. In: Corain B, Schmid G, Toshima N (eds) Metal nanoclusters in catalysis and materials science: the issue of size control. Elsevier, Hoboken, pp 149–166
2. Freund HJ, Shaikhutdinov S, Nilius N (2014) Model studies on heterogeneous catalysts at the atomic scale. Top Catal 57:822–832
3. Ertl G (2008) Reactions at surfaces: from atoms to complexity (Nobel Lecture). Angew Chem Int Ed 47:3524–3535
4. Spiel C, Vogel D, Schlögl R, Rupprechter G, Suchorski Y (2015) Spatially coupled catalytic ignition of CO oxidation on Pt: mesoscopic versus nano-scale. Ultramicroscopy 159:178–183 **and references therein**
5. Vogel D, Spiel C, Suchorski Y, Trinchero A, Schlögl R, Grönbeck H, Rupprechter G (2012) Local light-off in catalytic CO oxidation on low-index Pt and Pd surfaces: a combined PEEM, MS and DFT study. Angew Chem Int Ed 51:10041–10044
6. Bennett RA, Jones IZ, Bowker M (2007) CO oxidation studied using 'fast' XPS and a molecular beam reactor. Top Catal 42:373–376

7. Grunwaldt JD, Schroer CG (2010) Hard and soft X-ray microscopy and tomography in catalysis: bridging the different time and length scales. Chem Soc Rev 39:4741–4753
8. Beale AM, Jacques SDM, Weckhuysen BM (2010) Chemical imaging of catalytic solids with synchrotron radiation. Chem Soc Rev 39:4656–4672
9. Xie M, Freund HJ (2018) Optimal reactor design and operation taking catalyst deactivation into account. Chem Eng Sci 175:405–415
10. Shelef M, McCabe RW (2000) Twenty-five years after introduction of automotive catalysts: what next? Cat Today 62:35–50
11. Engel T, Ertl G (1978) A molecular beam investigation of the catalytic oxidation of CO on Pd (111). J Chem Phys 69:1267–1281
12. Somorjai GA (1979) Catalysis and surface science. Surf Sci 89:496–524
13. Gorodetskii VV, Nieuwenhuys BE (1981) Chemisorption and dissociation of carbon monoxide on rhodium surfaces. Surf Sci 105:299–312
14. Nieuwenhuys BE (1983) Adsorption and reactions of CO, NO, H_2 and O_2 on group VIII metal surfaces. Surf Sci 126:307–336
15. Kruse N, Abend G, Block JH (1984) Modelluntersuchungen zur Reaktion von CO und H_2 an Kobalt mittels Felddesorption. Chem Ing Tech 56:610–611
16. Cocke DL, Abend G, Block JH, Kruse N (1985) Oxidation of ruthenium studied by pulsed field desorption mass spectrometry. Langmuir 1:507–509
17. Gorodetskii V, Block JH, Drachsel W, Ehsasi M (1993) Oscillations in the carbon monoxide oxidation on platinum surfaces observed by field electron microscopy. Appl Surf Sci 67:198–205
18. Suchorski Y, Drachsel W (2007) Catalytic reactions on platinum nanofacets: bridging the size and complexity gap. Top Catal 46:201–215
19. Suchorski Y, Bespalov I, Zeininger J, Raab M, Datler M, Winkler P, Rupprechter G (2020) CO Oxidation on stepped Rh surfaces: µm-scale versus nanoscale. Cat Lett 150:605–612
20. Gorodetskii V, Lauterbach J, Rotermund HH, Block JH, Ertl G (1994) Coupling between adjacent crystal planes in heterogeneous catalysis by propagating reaction-diffusion waves. Nature 370:276–279
21. De Bocarmé TV, Beketov G, Kruse N (2004) Water formation from O_2 and H_2 on Rh tips: studies by field ion microscopy and pulsed field desorption mass spectrometry. Surf Interface Anal 36:522–527
22. Barroo C, Lambeets SV, Devred F, Chau TD, Kruse N, De Decker Y, De Bocarmé TV (2014) Hydrogenation of NO and NO_2 over palladium and platinum nanocrystallites: case studies using field emission techniques. New J Chem 38:2090–2097
23. De Bocarmé TV, Kruse N (2011) Field emission techniques for studying surface reactions: applying them to NO-H_2 interaction with Pd tips. Ultramicroscopy 111:376–380
24. Barroo C, De Decker Y, De Bocarmé TV (2017) NO_2 hydrogenation on Rh catalysts: bifurcations and oscillations at the nanoscale. J Phys Chem C 121:17235–17243
25. Barroo C, Bagot PAJ, Smith GDW, De Bocarmé TV (2014) Investigating nano-structured catalysts at the atomic scale by field ion microscopy and atom probe tomography. In: Hermans S, De Bocarmé TV (eds) RSC catalysis series: atomically-precise methods for synthesis of solid catalysts. RSC, London, pp 248–295
26. Lambeets SV, De Bocarmé TV, Perea DE, Kruse N (2020) Directional gateway to metal oxidation: 3D chemical mapping unfolds oxygen diffusional pathways in rhodium nanoparticles. J Phys Chem Lett 11:3144–3151
27. Suchorski Y, Beben J, James EW, Evans JW, Imbihl R (1999) Fluctuation-induced transitions in a bistable surface reaction: Catalytic CO oxidation on a Pt field emitter tip. Phys Rev Lett 82:1907–1910
28. Suchorski Y, Beben J, Imbihl R, James EW, Liu DJ, Evans JW (2001) Fluctuations and critical phenomena in catalytic CO oxidation on nanoscale Pt facets. Phys Rev B 63(1–12):165417
29. Suchorski Y, Rupprechter G (2018) Heterogeneous surfaces as structure and particle size libraries of model catalysts. Catal Lett 148:2947–2956
30. Suchorski Y, Rupprechter G (2016) Local reaction kinetics by imaging. Surf Sci 643:52–58
31. Lauterbach J, Rotermund HH (1994) Gas-phase coupling in the CO oxidation reaction on polycrystalline platinum. Cat Lett 27:27–32
32. Spiel C, Vogel D, Suchorski Y, Drachsel W, Schlögl R, Rupprechter G (2011) Catalytic CO oxidation on individual (110) domains of a polycrystalline Pt foil: local reaction kinetics by PEEM. Cat Lett 141:625–632
33. Datler M, Bespalov I, Buhr S, Zeininger J, Stöger-Pollach M, Bernardi J, Rupprechter G, Suchorski Y (2016) Hydrogen oxidation on stepped Rh Surfaces: µm-scale versus nanoscale. Cat Lett 146:1867–1874
34. Suchorski Y, Schmidt W, Ernst N, Block JH, Kreuzer H (1995) Electrostatic fields above individual atoms. Prog Surf Sci 48:121–134
35. Smoluchowski R (1941) Anisotropy of the electronic work function of metals. Phys Rev 60:661–674
36. Müller EW, Tsong TT (1969) Field ion microscopy, principles and applications. Elsevier, New York
37. Suchorski Y (2018) Field ion and field desorption microscopy: surface chemistry applications. In: Wandelt K (ed) Encyclopedia of interfacial chemistry—surface science and electrochemistry. Experimental methods, vol 1.1. Elsevier, New York, pp 162–179
38. Kreuzer HJ, Wang RLC (1997) Resonant field ionization: a new imaging mechanism in the field ion microscope. Z Phys Chem 202(1–2):127–138
39. Winkler P, Zeininger J, Raab M, Rupprechter G, Suchorski Y (2020) A novel wireless sample temperature control system for field ion, field electron, and atom probe techniques. Rev Sci Instrum 91(1):013705-1-7
40. Gong C, Huang K, Deng B, Liu X (2011) Catalyst light-off behavior of a spark-ignition LPG (liquefied petroleum gas) engine during cold start. Energy 36(1):53–59 **and references therein**
41. Frank-Kamenetskii DAB (1969) Appleton JP (transl. ed.) Diffusion and heat transfer in chemical kinetics. (2nd ed.) Plenum Press, New York
42. Vogel D, Spiel C, Suchorski Y, Urich A, Schlögl R, Rupprechter R (2011) Mapping the local reaction kinetics by PEEM: CO oxidation on individual (100)-type grains of Pt foil. Surf Sci 605:1999–2005
43. Suchorski Y, Spiel C, Vogel D, Drachsel W, Schlögl R, Rupprechter G (2010) Local reaction kinetics by imaging: CO oxidation on polycrystalline platinum. ChemPhysChem 11(2010):3231–3235
44. Knight B, Sirovich L (1990) Kolmogorov inertial range for inhomogeneous turbulent flows. Phys Rev Lett 65:1356–1359
45. Ciliberto S, Nicolaenko B (1991) Estimating the number of degrees of freedom in spatially extended systems. Europhys Lett 14:303–312
46. Suchorski Y, Beben J, Imbihl R (2000) Spatiotemporal dynamics of fluctuations in a surface reaction by Karhunen-Loeve decomposition of field emission images. Surf Sci 454–456:331–336
47. Bagyan S, Mair T, Suchorski Y, Hauser M, Straube R (2008) Spatial desynchronization of glycolytic waves as revealed by Karhunen– Loève analysis. J Phys Chem B 112:14334–14341
48. Seebauer EG, Allen CE (1995) Estimating surface diffusion coefficients. Progr Surf Sci 49:265–330
49. Beben J, Suchorski Y (2003) Surface diffusion by adsorbate density fluctuation measurements. Progr Surf Sci 74:3–24 **and references therein**

50. Vogel D, Spiel C, Schmid M, Stöger-Pollach M, Schlögl R, Suchorski Y, Rupprechter G (2013) The role of defects in the local reaction kinetics of CO oxidation on low-index Pd surfaces. J Phys Chem C 117:12054–12060
51. Somorjai GA (1985) Surface science and catalysis. Science 227(4689):902–908
52. Tian N, Zhou ZY, Sun SG (2008) Platinum metal catalysts of high-index surfaces: from single-crystal planes to electrochemically shape-controlled nanoparticles. J Phys Chem C 112:19801–19817
53. BASF Automotive Solutions (2019) Three automotive sustainability challenges facing the Industry. Retrieved May 04, 2020, from https://automotive.basf.com/news/read/3-automotive-sustainability-challenges-facing-the-industry
54. Carrette L, Friedrich KA, Stimming U (2000) Fuel cells: principles, types, fuels, and applications. ChemPhysChem 1:162–193
55. Hopstaken MJP, Niemantsverdriet JW (2000) Structure sensitivity in the CO oxidation on rhodium: effect of adsorbate coverages on oxidation kinetics on Rh (100) and Rh (111). J Chem Phys 113:5457–5465
56. Gao F, Cai Y, Gath KK, Wang Y, Chen MS, Guo QL, Goodman DW (2009) CO oxidation on Pt-group metals from ultrahigh vacuum to near atmospheric pressures. 1. Rhodium J Phys Chem C 113:182–192
57. Kizilkaya AC, Gracia JM, Niemantsverdriet JW (2010) A direct relation between adsorbate interactions, configurations, and reactivity: CO oxidation on Rh (100) and Rh (111). J Phys Chem C 114:21672–21680
58. Bowker M, Guo Q, Li Y, Joyner RW (1993) Structure sensitivity in CO oxidation over rhodium. Catal Lett 18:119–123
59. Goodman DW, Peden CHF, Fisher GB, Oh SH (1993) Comment on "Structure sensitivity in CO oxidation over rhodium" by M. Bowker, Q. Guo, Y. Li and R.W. Joyner Catal Lett 22:271–274
60. Bowker M, Guo Q, Li Y, Joyner RW (1993) Structure sensitivity of CO oxidation over rhodium. Reply to comments by Fisher, Peden, Oh and Goodman. Catal Lett 22:275–276
61. Johansson S, Österlund L, Kasemo B (2001) CO oxidation bistability diagrams for Pt/CeO_x and Pt/SiO_2 model catalysts prepared by electron-beam lithography. J Catal 201(2):275–285
62. Berdau M, Yelenin GG, Karpowicz A, Ehsasi M, Christmann K, Block JH (1999) Macroscopic and mesoscopic characterization of a bistable reaction system: CO oxidation on Pt (111) surface. J Chem Phys 110(23):11551–11573
63. Rose KC, Battogtokg D, Mikhailov A, Imbihl R, Engel W, Bradshaw AM (1996) Cellular structures in catalytic reactions with global coupling. Phys Rev Lett 76(19):3582–3585
64. Falta J, Imbihl R, Henzler M (1990) Spatial pattern formation in a catalytic surface reaction: the facetting of Pt(110) in $CO+O_2$. Phys Rev Lett 64(12):1409–14012
65. Liu DJ, Evans JW (2009) Atomistic and multiscale modeling of CO-oxidation on Pd (1 0 0) and Rh (1 0 0): from nanoscale fluctuations to mesoscale reaction fronts. Surf Sci 603(10–12):1706–1716
66. Leibsle FM, Murray PW, Francis SM, Thornton G, Bowker M (1993) One-dimensional reactivity in catalysis studied with the scanning tunnelling microscope. Nature 363(6431):706–709
67. Suchorski Y, Kozlov SM, Bespalov I, Datler M, Vogel D, Budinska Z, Neyman KM, Rupprechter G (2018) The role of metal/oxide interfaces for long-range metal particle activation during CO oxidation. Nat Mater 17(6):519–522 **and references therein**
68. Schiller F, Ilyn M, Perez-Dieste V, Escudero C, Huck-Iriart C, Del Arbol NR, Hagman B, Merte LR, Bertram F, Shipilin M, Blomberg S, Gustafson J, Lundgren E, Ortega JE (2018) Catalytic oxidation of carbon monoxide on a curved Pd crystal: spatial variation of active and poisoning phases in stationary conditions. J Am Chem Soc 140:16245–16252
69. Belton DN, Fischer GB, Gl DiMaggio (1990) Identification of molecular and subsurface oxygen on stepped Rh(711). Surf Sci 233:12–26
70. Mittendorfer F, Seriani N, Dubay O, Kresse G (2007) Morphology of mesoscopic Rh and Pd nanoparticles under oxidizing conditions. Phys Rev B 76:233413-1–233414
71. Koch HP, Singnurkar P, Schennach R, Stroppa A, Mittendorfer F (2008) A RAIRS, TPD, and DFT study of carbon monoxide adsorption on stepped Rh(553). J Phys Chem C 112:806–812

Publisher's Note Springer Nature remains neutral with regard to jurisdictional claims in published maps and institutional affiliations.